Unraveling the flow of information in a nonequilibrium process in the presence of hydrodynamic interactions

Biswajit Das,[1,*] Sreekanth K. Manikandan,[2,†] and Ayan Banerjee[1,‡]

[1] *Department of Physical Sciences, Indian Institute of Science Education and Research Kolkata, Mohanpur Campus, Mohanpur, West Bengal, 741246, India*

[2] *Department of Physics, Gothenburg University, Gothenburg, Sweden*

(Received 5 May 2025; revised 23 July 2025; accepted 26 August 2025; published 16 September 2025)

Identifying the origin of nonequilibrium characteristics in a generic interacting system having multiple degrees of freedom is a challenging task. In this context, information-theoretic measures such as mutual information and related polymorphs offer valuable insights. Here we explore these measures in a minimal experimental model consisting of two hydrodynamically coupled colloidal particles, where a nonequilibrium drive is introduced via an exponentially correlated noise acting on one of the particles. We show that the information-theoretic tools considered enable a systematic, data-driven dissection of information flow within the system. These measures allow us to identify the driving node and reconstruct the directional dependencies between particles. Notably, they help explain a recently observed, counterintuitive trend in the dependence of irreversibility on interaction strength under coarse-graining [Das et al., Phys. Rev. E 112, L023401 (2025)]. Finally, our results demonstrate how directional information measures can uncover the hidden structure of nonequilibrium dynamics and provide a framework for studying similar effects in more complex systems.

DOI: 10.1103/dvb3-b2v8

I. INTRODUCTION

Understanding how interactions shape dynamics and thermodynamics in complex mesoscopic systems remains a central challenge in nonequilibrium physics [1–4]. When such systems operate far from equilibrium, especially in high-dimensional settings, interactions—both internal and environmentally mediated—can lead to emergent behaviors not directly predictable from individual components [5,6]. These emergent features include collective motion [6,7], pattern formation [8,9], and selective amplification of certain pathways or states [10,11]. In realistic settings, the environment introduces additional couplings between subsystems, often with memory or spatial correlations, complicating the interpretation of dynamical dependencies [7,12–14]. This makes it particularly difficult to isolate the origin of nonequilibrium driving or to identify which variables act as effective degrees of freedom in generating or transmitting nonequilibrium features. A fundamental open question, therefore, is: How can one systematically disentangle internal dynamics from environmental influences to identify the true source of irreversibility and driving within complex systems?

Recent developments in information theory have provided promising tools to address this. A prominent measure is mutual information, which quantifies the statistical dependencies between variables [15,16]. This has been successfully used to quantify interactions in mesoscopic systems, both at and away from equilibrium [17]. Extensions of this idea have been applied to systems having separable environmental and internal couplings [18,19], and to investigate interference effects arising from overlapping interactions [20]. However, mutual information is a symmetric and time-independent measure for a stationary process and does not capture the directional or dynamical properties, limiting its ability to reveal causal driving or flow of information—both of which are central in understanding nonequilibrium functionality.

Directionality becomes especially important in biological systems, where the ability to channel and route information is often essential for function. For example, signal processing in gene regulatory networks relies not just on correlations but also on well-defined causal structures [21,22]. To address this, time-delayed information measures, such as time-delayed mutual information [23–25] and transfer entropy [26–28], have emerged as powerful tools for uncovering directed dependencies from time-series data. These measures enable us to identify driving variables, causal directionality, and the locus of

*Contact author: bd18ip005@iiserkol.ac.in
†Contact author: sreekanth.manikandan@physics.gu.se
‡Contact author: ayan@iiserkol.ac.in

nonequilibrium activity—even in the presence of complex interactions [29–37].

To explore these ideas in a controlled setting, we consider a well-characterized mesoscopic system: two colloidal particles hydrodynamically coupled and confined in separate harmonic traps. While the hydrodynamic interaction couples their dynamics, the particles remain statistically independent in equilibrium [38]. However, when one of the traps is driven by exponentially correlated noise (modeled via an Ornstein-Uhlenbeck process), the system is driven out of equilibrium, and directional effects emerge. This kind of active noise can be seen as a stand-in for biochemical or environmental fluctuations with memory—akin to stimuli from an active bath [39–41].

In a recent study, we demonstrated a rather counterintuitive interplay between irreversibility (measured by the total entropy production rate [42–47]) and interactions in this system [48]. Specifically, we showed that increasing the interaction strength by reducing the distance between particles lowers the total irreversibility of the entire system. However, when we focus on coarse-grained subspaces that include only the particles (excluding the active drive), the trend reverses: the measured irreversibility increases with interaction strength. This presents an apparent conundrum—would the degree of coarse-graining performed dictate the nature of irreversibility? Here we use information-theoretic measures as tools to pinpoint the driving node, reconstruct the causal structure between subsystems, and quantify how hydrodynamic interactions shape both the directionality of information flow and, crucially, the emergence of this counterintuitive behavior.

The article is structured as follows: In Sec. II, we present a short overview of the theoretical framework of information-theoretic measures that we are interested in computing. Then we describe our experimental system in brief in Sec. III. In Sec. IV, we estimate information-theoretic measures from experimental and numerical trajectories and discuss our observations. Finally, we present our conclusions in Sec. V.

II. THEORETICAL FORMALISM: INFORMATION-THEORETIC MEASURES

Our focus of attention in this work lies in understanding the effect of interaction shaping the mutual dependence and, more importantly, the causal directionality of interactions between different degrees of freedom of a stochastic system. To comprehend the basic theoretical formalism we have adopted, consider—for simplicity—a generic system in a steady state with three interacting subsystems or variables x, y, and z with nearly identical spatiotemporal trajectories [Fig. 1(a)]—the extension to higher-dimensional systems is straightforward. Recent studies have shown that information-theoretic measures can be used to inspect both plausible mutual dependencies and causal relationships between these variables, in a data-driven manner [Fig. 1(b)]. We begin by introducing the measures that we consider in this study.

The mutual information (in the unit of *bits*) between any two continuous stochastic variables $x(t)$ and $y(t)$ is defined as [15,16]

$$MI_{xy} = \int dxdy\; P_{xy}(x,y) \log_2 \frac{P_{xy}(x,y)}{P_x(x)P_y(y)}, \qquad (1)$$

which is the Kullback-Leibler divergence between the joint distribution $P_{xy}(x,y)$ and the product of corresponding marginals $P_x(x)$ and $P_y(y)$. By definition, $MI_{xy} \geq 0$ and $MI_{xy} = 0$ only when the variables are independent. Recently, mutual information has been widely used in stochastic processes to understand the effects of complex environments [18,19] and the role of activity [20,50], even in several biological phenomena such as cell signaling [51–53] and neuronal signal processing [54,55]. It has also been used as a measure to quantify the distance between two distributions in nonequilibrium transformations [56–59]. In this most basic form, by construction, MI_{xy} is a symmetric and time-independent quantity, and thereby is incapable of detecting any causal characteristics or dynamics of information transfer from one state to another. In this context, two other information-theoretic measures—time-delayed mutual information and transfer entropy—have been proposed. We now turn our attention to these entities.

The time-delayed mutual information from the variable x to the variable y is defined as [23–25]

$$\begin{aligned} MI_{x\rightarrow y}(\tau) &= \int dx_t dy_{t+\tau}\; P_{xy}(x_t, y_{t+\tau}) \log_2 \frac{P_{xy}(x_t, y_{t+\tau})}{P_x(x_t)P_y(y_{t+\tau})} \\ &\equiv \int dx_t dy_{t+\tau}\; P_{xy}(x_t, y_{t+\tau}) \log_2 \frac{P_{xy}(y_{t+\tau}|x_t)}{P_y(y_{t+\tau})}, \end{aligned} \qquad (2)$$

where τ denotes the finite time lag between the two variables. This quantity essentially measures mutual information between two segments of trajectories that are time-delayed with respect to each other, such as $x_t \equiv (x^1, x^2, \ldots, x^{n-m})$ and $y_{t+\tau} \equiv (y^{1+m}, y^{2+m}, \ldots, y^n)$. Here, n denotes the block of trajectory length up to a fixed time t, and $m = \tau/\Delta t$ denotes the number of points corresponding to a time delay τ. Note that we compute the mutual information between these finite segments, not between entire stochastic trajectories in the pathwise sense [60]. Unlike steady-state mutual information, its time-delayed version is asymmetric in general, i.e., $MI_{x\rightarrow y}(\tau) \neq MI_{y\rightarrow x}(\tau)$. Furthermore, since its structure is explicitly lag time dependent, it can be leveraged to detect the effective directional information transfer in (x,y) phase space.

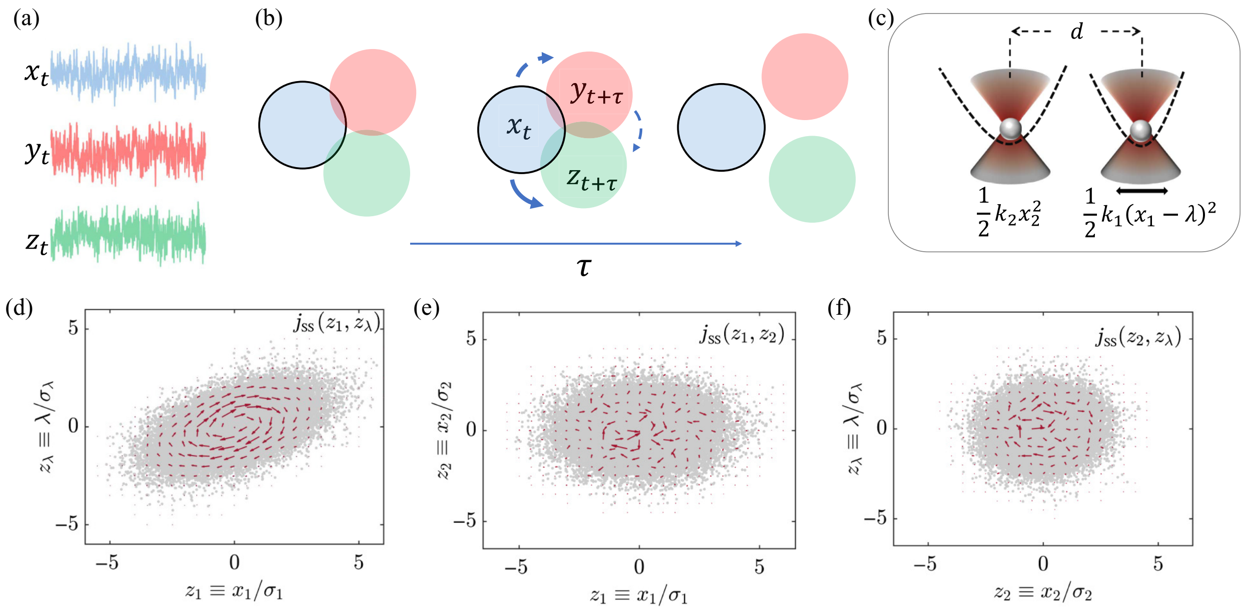

FIG. 1. (a) Spatiotemporal trajectories corresponding to the three interacting variables x, y, and z of a generic system. (b) The mutual dependence of these variables is also a function of the lag time τ. The extent of overlap at intermediate τ is informative of the causal directionality indicated by the arrows. We can establish such causal structure between the variables by estimating information-theoretic measures [23,26]. (c) Experimental system consisting of two hydrodynamically coupled microparticles trapped in two optical traps separated by distance d. The mean position of the trap with stiffness constant k_1 is modulated by the Ornstein-Uhlenbeck noise $\lambda(t)$, while the other trap (with stiffness constant k_2) remains fixed. The fluctuating positions of the particles with respect to the center of each optical trap are denoted by $x_1(t)$ and $x_2(t)$. (d)–(f) Probability currents ($j_{\rm ss}$) [48,49] (shown as maroon arrows) computed from experimentally recorded spatiotemporal trajectories in every bivariate subspace of our system in the presence of external *active* drive. The dynamical variables (x_1, x_2, λ) are normalized to make them dimensionless. Here $\sigma_1 = \sqrt{k_BT/k_1}$, $\sigma_2 = \sqrt{k_BT/k_2}$, and $\sigma_\lambda = \sqrt{D_e/\tau_e}$.

A nonzero value of the time-delayed mutual information as a function of τ indicates causal interactions between two variables. For a generic stationary process, it can be shown that $MI_{x\to y}(-\tau) = MI_{y\to x}(\tau)$, suggesting that while $MI_{x\to y}(\tau)$ quantifies how the present x_t predicts the future $y_{t+\tau}$, for a negative lag, this simply swaps to how the present y_t predicts the future $x_{t+\tau}$. The sign of the time lag $\tau^{\max}$ at which this quantity reaches its peak magnitude (global maximum) can then be used to infer the direction of information flow [25]. Hence, a positive $\tau_{\max}$ in Eq. (2) indicates that y shares maximum information with the past of x, which implies that x drives y. Also, if $MI_{x\to y}(\tau) > MI_{y\to x}(\tau)$, it can be statistically considered that the information is predominantly shared from the variable (or process) x to the variable y and not the other way around [24].

However, it is important to point out that time-delayed mutual information measures only the difference between $P_{xy}(y_{t+\tau}|x_t)$ and $P_y(y_{t+\tau})$—which quantifies the reduction in uncertainty regarding the future of y, thereby incorporating the history of x. By definition, it does not exclude the effects induced by its own (y) history [24]. To remove this effect, another time-dependent measure—the transfer entropy—was introduced by Schreiber [26].

The transfer entropy is defined as [26–28]

$$TE_{x\to y}(\tau) = \int dx_t dy_t dy_{t+\tau}\, P_{xy}(y_{t+\tau}, y_t, x_t) \log_2 \frac{P_{xy}(y_{t+\tau}|y_t, x_t)}{P_y(y_{t+\tau}|y_t)}. \tag{3}$$

This quantity basically measures the reduction of uncertainty regarding the present value of y by knowing the history of x, given that the history of y is known as well. Unlike time-delayed mutual information, transfer entropy is argued to exclude the variable's own history, and thereby captures purely exchanged information between the subsystems. This measure is also asymmetric by construction as $TE_{x\to y}(\tau) \neq TE_{y\to x}(\tau)$, which is suggestive of a prominent direction of information flow. Furthermore, if $TE_{x\to y}(\tau) \gg TE_{y\to x}(\tau)$, the evidence of (causal) directional influence from the process x to the process y can be statistically ensured [28]. Note that for negative time lags, $TE_{x\to y}(-\tau)$ sets conditions on the future of the target, so it does not follow the simple sign-flip symmetry of time-delayed mutual information. As a result, $TE_{x\to y}(-\tau)$ does not generally equal $TE_{y\to x}(\tau)$. It is also expected that the standard positive-lag transfer entropy remains more directly meaningful for causal interpretation.

Both these quantities are used in various domains to understand the causal connection and structure of connectivity between different variables [24,30,33,34]. For example, time-delayed mutual information was used to explore spatiotemporal information transport in physical systems [23] and to infer causal interactions in neural network systems [61] and chaotic systems [62]. On the other hand, transfer entropy is typically used to understand the information flows within gene regulatory networks [21,22], in biochemical signaling [33], and in various other systems characterized by long memory [63,64]. More recently, such measures have also been used to reconstruct a directed graph for a system with many interacting dynamical variables that are spatially separated [28]. In an alternative context, the rates of such quantities are also used to derive a generalized second law of information thermodynamics for systems without bipartite structure [36]. Moreover, the connection between such information-theoretic measures (particularly transfer entropy) and the response in a spatially asymmetric extended system has also been explored [65,66].

Given the unique advantages of information-theoretic measures, we seek to apply these tools to our experimental nonequilibrium system, where hydrodynamic interactions are prevalent. The system consists of two colloidal particles in two separate harmonic traps, placed in very close separation so that hydrodynamic interactions naturally arise [Fig. 1(c)]. In addition, one of the particles is driven by an external stochastic protocol, which makes the overall process nonequilibrium, characterized by probability fluxes [48,49] in different phase spaces [Figs. 1(d)–1(f)]. Unlike conventional interactions of conservative origin, hydrodynamic interactions are dissipative and can, in certain cases, intrinsically link both deterministic and stochastic forces acting on the interacting degrees of freedom [38]. This leads to an emergent *non-multipartite* structure [67] in the dynamics. It turns out that such a dissipative and multipartite structure significantly influences the irreversibility and entropy production of this system.

In previous work, we showed that, rather counterintuitively, increasing the interaction strength (by bringing the two colloidal particles closer to each other) reduces overall irreversibility and entropy production in this process, but at the level of coarse-grained subspaces—comprising only the particles—this trend reverses [48]. We were able to verify this trend over all possible ranges of parameter values for this system, both experimentally and with exact analytical solutions of the corresponding Langevin model. This raises a fundamental question: What underlying dynamical dependencies drive these opposing trends in entropy production at different levels of description, and how do they shape the spatiotemporal structure of irreversibility in the system?

Here we address this question by using the aforementioned information-theoretic tools on both the experimental data and the numerical data of this system. We demonstrate that these tools systematically dissect the role of hydrodynamic interactions in establishing dependencies between dynamical variables across all relevant phase planes, and then go on to show how these dependencies evolve over time such that causal connections emerge between them. Crucially, they capture the apparent contradiction in irreversibility trends across different levels of description, providing a coherent framework for understanding nonequilibrium behavior in hydrodynamically coupled systems. We also discuss the interplay between hydrodynamic interactions and the strength of external driving in shaping the information flow in the full phase space.

III. EXPERIMENTAL MODEL

Our system consists of two identical Brownian particles confined in two separate harmonic traps at close separation in a viscous fluid. Experimentally, the system is realized with the optical tweezers created by the tight focusing of two perpendicularly polarized Gaussian beams emanating from two solid-state lasers of wavelength 1064 nm. To manifest a nonequilibrium scenario, the mean position of one of the traps is modulated by a correlated noise $\lambda(t)$ with correlation timescale τ_e—following an Ornstein-Uhlenbeck process such that $\langle\lambda(t)\lambda(t')\rangle = (D_e/\tau_e)\exp(-(t-t')/\tau_e)$ [68]. One of the beams is passed through an acousto-optic modulator so as to add an external Ornstein-Uhlenbeck noise. Then the position fluctuations of both particles are separately recorded at a rate of 10 kHz for 50 s with the use of a "balanced-detector-system" consisting of high-gain photodiodes. Further details about the experiment can be found in Ref. [48].

The dynamics of the microparticles, which are at close separation, is coupled via hydrodynamic interaction of strength $\epsilon = (3a/2d) - (a/d)^3$, where d is the separation between the mean positions of the traps and a denotes the radius of the particle ($a = 1.5$ μm). In some ways, this system can be mirrored as a biochemical channel with two nodes, where one of the nodes has access to additional *active* fluctuations acting as an external signal [69]. A schematic of the system is illustrated in Fig. 1(c). Theoretically, the system with the particles trapped in optical potentials with different stiffness constants k_1 and k_2 can be expressed with coupled, linear *Langevin* equations [48]:

$$\begin{aligned}
\dot{x}_1(t) &= \mathcal{H}_{11}[-k_1(x_1(t)-\lambda(t))+\xi_1(t)] \\
&\quad + \mathcal{H}_{12}[-k_2x_2(t)+\xi_2(t)], \\
\dot{x}_2(t) &= \mathcal{H}_{21}[-k_1(x_1(t)-\lambda(t))+\xi_1(t)] \\
&\quad + \mathcal{H}_{22}[-k_2x_2(t)+\xi_2(t)], \\
\dot{\lambda}(t) &= -\lambda(t)/\tau_e + \sqrt{2D_e}/\tau_e\eta_3(t),
\end{aligned} \tag{4}$$

where $\mathcal{H}_{ij}$ $(i,j = 1,2)$ are the constant elements of a hydrodynamic coupling tensor of the form $\mathcal{H} = \begin{pmatrix} 1/\gamma & \epsilon/\gamma \\ \epsilon/\gamma & 1/\gamma \end{pmatrix}$—considering that the displacements of the particles (measured with respect to the center of the corresponding trap)—denoted as $x_1(t)$ and $x_2(t)$—are small compared with the mean separation d between the traps, and $\gamma \equiv 6\pi\eta a$ is the viscous drag coefficient of the medium [70]. The terms $\xi_1(t)$ and $\xi_2(t)$ are δ-correlated random Brownian forces such that $\langle\xi_i(t)\rangle = 0$ and $\langle\xi_i(t)\xi_j(t)\rangle = 2k_BT(\mathcal{H})^{-1}_{ij}\delta(t-t')$, where k_B is Boltzmann's constant. Additionally, $\langle\eta_3(t)\rangle = 0$, $\langle\eta_3(t)\eta_3(t')\rangle = \delta(t-t')$, and $\langle\xi_1(t)\eta_3(t')\rangle = \langle\xi_2(t)\eta_3(t')\rangle = 0$. Equation (4) can be rewritten as $\dot{\mathbf{x}}(t) = -\mathbf{F}\cdot\mathbf{x}(t) + \boldsymbol{\xi}(t)$, with $\mathbf{x}(t) = [x_1(t), x_2(t), \lambda(t)]^T$ and $\boldsymbol{\xi}(t) = [(\xi_1(t) + \epsilon\xi_2(t))/\gamma, (\epsilon\xi_1(t) + \xi_2(t))/\gamma, \eta_3(t)]^T \equiv [\eta_1(t), \eta_2(t), \eta_3(t)]^T$ such that $\langle\boldsymbol{\xi}(t) : \boldsymbol{\xi}(t')\rangle = 2\mathbf{D}\delta(t-t')$. The interaction matrix $\mathbf{F}$ and the diffusion matrix $\mathbf{D}$ are of the forms

$$\mathbf{F} = \begin{pmatrix} 1/\tau_1 & \epsilon/\tau_2 & -1/\tau_1 \\ \epsilon/\tau_1 & 1/\tau_2 & -\epsilon/\tau_1 \\ 0 & 0 & 1/\alpha\tau_1 \end{pmatrix}, \quad \mathbf{D} = \begin{pmatrix} D_0 & \epsilon D_0 & 0 \\ \epsilon D_0 & D_0 & 0 \\ 0 & 0 & \theta D_0 \end{pmatrix}, \tag{5}$$

where $\tau_1 = \gamma/k_1$, $\tau_2 = \gamma/k_2$, $\alpha = \tau_e/\tau_1$, $D_0 = k_BT/\gamma$, and $\theta = (D_e/\tau_e^2)/D_0$. In the experiment, $D_0 \sim 0.16$ $\mu\text{m}^2/\text{s}$, $\tau_1 \sim 1.5$ ms, $\tau_2 \sim 2.1$ ms, and $\tau_e = 4$ ms are fixed such that $\alpha \sim 2.7$. We vary the nonequilibrium strength by D_e such that θ varies from 0.14 to 0.56 at two different separations of the particles, corresponding to hydrodynamic interaction strengths ϵ of 0.49 and 0.29. Note that the diffusion matrix at any separation is nondiagonal, which is a characteristic feature in the case of hydrodynamic interactions as it encodes the fact that the noise acting on one particle is correlated with the motion of the other particle due to fluid-mediated couplings. The steady-state distribution of the system over the phase space defined by (x_1, x_2, λ) will be a multivariate Gaussian such that $P(x_1, x_2, \lambda) \sim \mathcal{N}(0, \mathbf{C}) \sim \exp(-\frac{1}{2}\mathbf{x}^T\mathbf{C}\mathbf{x})$, and the covariance matrix $\mathbf{C}$ can be computed by solving the Lyapunov equation: $\mathbf{FC} + \mathbf{CF}^T = 2\mathbf{D}$. The steady-state distribution of the system at marginal bivariate subspaces [i.e., (x_1, x_2), (x_1, λ), (x_2, λ)] will also be Gaussian. For example, $P(x_1, x_2) \sim \mathcal{N}(0, \mathbf{C}_{x_1x_2})$, where $\mathbf{C}_{x_1x_2}$ is a submatrix of $\mathbf{C}$ whose rows and columns correspond to x_1 and x_2. The elements of the steady-state covariance matrix $\mathbf{C}$ are explicitly shown in Appendix A.

IV. RESULTS AND DISCUSSION

A. Estimation of mutual information

We begin by estimating $MI_{\lambda x_1}$, $MI_{\lambda x_2}$, and $MI_{x_1x_2}$ as we aim to investigate how hydrodynamic interactions affect the interaction of the individual particles with the external drive as well as the coupling between the trapped particles under an external nonequilibrium drive. Because of the Gaussian features of $P_{x_1x_2}$ and its marginals, the mutual information between x_1 and x_2 can be analytically computed as [20,50]

$$MI_{x_1x_2} = \frac{1}{2}\log_2\frac{c_{x_1x_1}c_{x_2x_2}}{\det\mathbf{C}_{x_1x_2}}, \tag{6}$$

where $c_{x_1x_1}$ and $c_{x_2x_2}$ are the diagonal entries of the corresponding submatrix $\mathbf{C}_{x_1x_2}$ of the covariance matrix $\mathbf{C}$. Similarly, the mutual information between the external drive λ and the driven particle can be estimated as

$$MI_{\lambda x_1} = \frac{1}{2}\log_2\frac{c_{\lambda\lambda}c_{x_1x_1}}{\det\mathbf{C}_{\lambda x_1}}, \tag{7}$$

with use of the submatrix $\mathbf{C}_{\lambda x_1}$ and its diagonal entries. On the other hand, $MI_{\lambda x_2}$ can be similarly calculated with use of the submatrix $\mathbf{C}_{\lambda x_2}$. The analytical expressions for these quantities are explicitly shown in Appendix B. Moreover, the signature of nonzero mutual information will be encoded in the characteristic differences between the joint probability distribution of two variables and the product of the corresponding marginals. As we compare different joint probability distributions and the products of the marginals in Figs. 2(a)–2(c), it is clear that the mutual information between λ and x_1 will be significantly greater than the mutual information between x_1 and x_2 or λ and x_2. This is consistent with the fact that the active drive λ is directly applied to the mean position of the first trap so that the position fluctuations of the first particle x_1 get strongly affected by the drive, which leads to significantly stronger dependence between them. On the other hand, both the interparticle interaction and the connection between the second particle x_2 and the drive λ are mediated by hydrodynamic interaction, which leads to relatively weaker dependence.

We then use a k-nearest-neighbor (kNN) estimator [71] to compute mutual information between different variables from the experimental and numerical trajectories. The k-nearest-neighbor estimator relies on nonparametric methods to compute mutual information in a data-driven manner so that it naturally adapts to the local structure of the data distribution irrespective of the underlying probability distributions [72].

We find that the steady-state mutual information between the driven particle x_1 and the external drive λ is less at higher hydrodynamic interaction strength ϵ at any strengths θ of the nonequilibrium drive [Fig. 2(d)]. On the other hand, the mutual information between other dynamical variables ($MI_{x_1x_2}$ and $MI_{\lambda x_2}$) is indeed enhanced in the case of strong hydrodynamic interaction for any strength of the external drive, as shown in Figs. 2(e) and 2(f). These observations are nontrivial and suggest that the interactions with the other particle reduce the effect of the nonequilibrium drive that the first particle experiences as compared with the noninteracting limit. We can

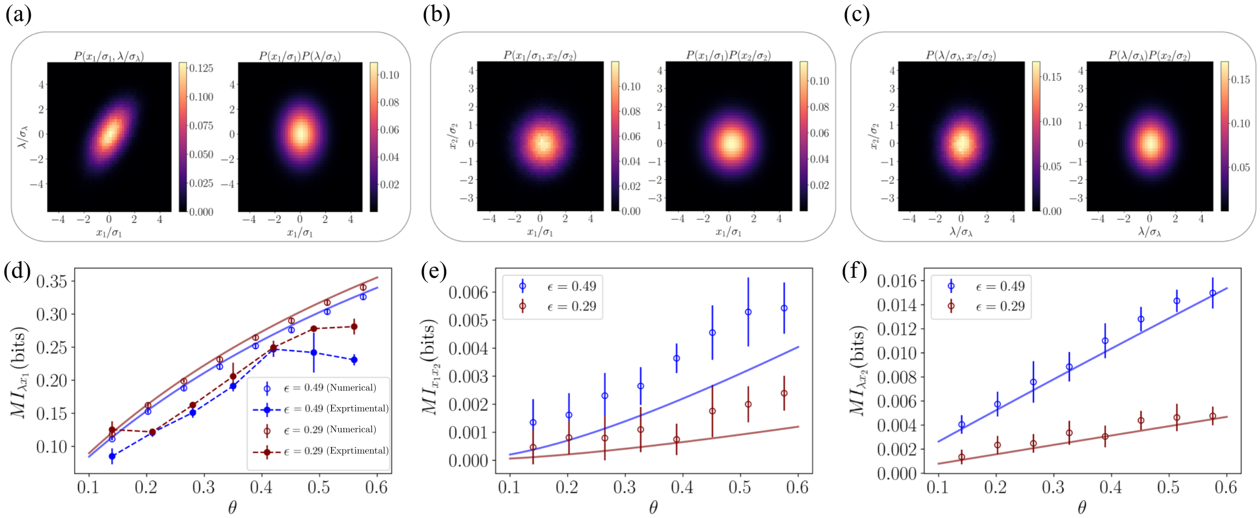

FIG. 2. System with hydrodynamic interaction. (a)–(c) Joint probability distribution functions of any two dynamical variables of the system [such as $P(\lambda, x_1)$, $P(x_1, x_2)$, and $P(\lambda, x_2)$] and the product of the corresponding marginals [such as $P(\lambda)P(x_1)$, $P(x_1)P(x_2)$, and $P(\lambda)P(x_2)$] for a particular nonequilibrium strength $\theta = 0.56$ and hydrodynamic interaction strength $\epsilon = 0.49$. The dynamical variables are normalized to make them dimensionless. Here $\sigma_1 = \sqrt{k_B T/k_1}$, $\sigma_2 = \sqrt{k_B T/k_2}$, and $\sigma_\lambda = \sqrt{D_e/\tau_e}$. (d)–(f) Mutual information between different dynamical variables at the steady-state estimated for different nonequilibrium noise strengths θ at two different interaction strengths ϵ. Here the open symbols denote the mutual information estimated from the numerical trajectories, and the filled symbols denote the same estimated from the experimental trajectories. $MI_{x_1x_2}$ and $MI_{\lambda x_2}$ are estimated only from the numerical trajectories as the expected values (for the regimes of experimental parameters) are too low and may be overwhelmed by the noise level of the experiment. The solid lines represent corresponding analytical estimations. Details of the numerical simulations of the model are provided in Appendix C.

indeed trace back the decrease in the total entropy production rate to this observation. Additionally, the enhancement of mutual information between the particles ($MI_{x_1x_2}$) at higher interaction strengths also corroborates our previous observation related to the trend of irreversibility in the coarse-grained phase space [48].

B. Time-delayed information measures

We show that the mutual information successfully captures the effect of the hydrodynamic interactions in building the mutual dependencies between the dynamical variables of each phase plane. Still, it is not enough to pinpoint the dominant variable that drives the dynamics of the other variable in a phase plane, which means that the dynamics or direction of information flow remains unknown. Since directional information flow indicates the direction of interactions between local subsystems—which may have impacts on the overall dynamical and thermodynamical properties of the system—we next compute time-delayed mutual information [as defined in Eq. (2)] between different dynamical variables to understand the possible directional dependencies in our system.

Similarly to what we did for the time-independent mutual information, we compute mutual information between two variables using the k-nearest-neighbor estimator [71], but now with a pair of variables where one among them lags behind the other with lag time τ. In other words, we compute different combinations of mutual information from the time-delayed experimental and numerical trajectories. Specifically, we estimate the time-delayed mutual information parameters $MI_{\lambda\to x_1}(\tau)$, $MI_{x_1\to x_2}(\tau)$, and $MI_{\lambda\to x_2}(\tau)$ along with their reverse counterparts to determine the directionality of information flow.

The time-delayed mutual information turns out to be asymmetric under the change of arguments. As we show in Fig. 3, for nonequilibrium strength $\theta = 0.56$ and hydrodynamic interaction strength $\epsilon = 0.49$, $MI_{\lambda\to x_1}(\tau) > MI_{x_1\to\lambda}(\tau)$, $MI_{x_1\to x_2}(\tau) > MI_{x_2\to x_1}(\tau)$, and $MI_{\lambda\to x_2}(\tau) > MI_{x_2\to\lambda}(\tau)$, which strongly indicates the preferred direction of information flow. Additionally, $MI_{\lambda\to x_1}(\tau)$, $MI_{x_1\to x_2}(\tau)$, and $MI_{\lambda\to x_2}(\tau)$ have global maxima at different time lags. While two of the reverse counterparts, $MI_{x_1\to\lambda}(\tau)$ and $MI_{x_2\to\lambda}(\tau)$, do not possess any such maxima, $MI_{x_2\to x_1}(\tau)$ shows a maximum at a particular time lag, similarly to $MI_{x_1\to x_2}(\tau)$. The presence of a maximum in $MI_{x_2\to x_1}(\tau)$ indicates that there is a possibility of information backflow from the fixed particle x_2 to the driven particle x_1. On the other hand, the exponential-type decay that appears in $MI_{x_1\to\lambda}(\tau)$ and $MI_{x_2\to\lambda}(\tau)$ is due to the inherent nature of time-delayed mutual information, where it fails to exclude the effects induced due to the history of λ (which is exponentially correlated), as can be understood from the second definition

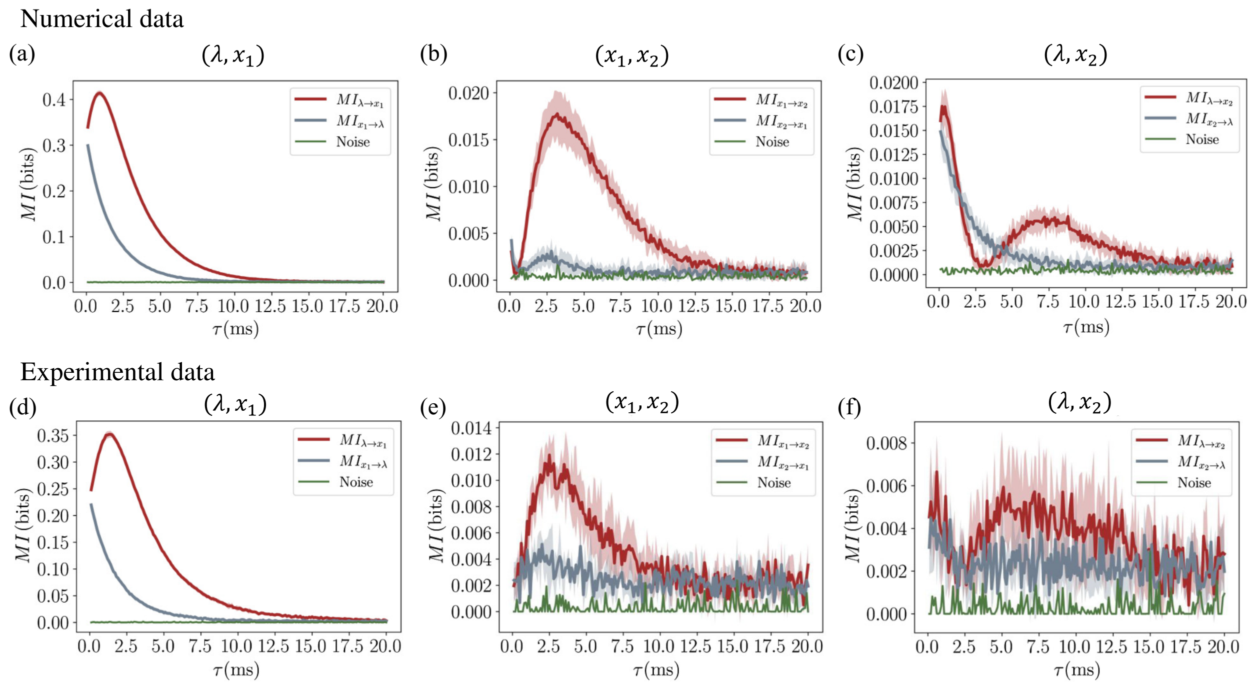

FIG. 3. Estimated time-delayed mutual information between different dynamic variables of the system with $\theta = 0.56$ and $\epsilon = 0.49$ in (a),(d) (λ, x_1) space, (b),(e) (x_1, x_2) space, and (c),(f) (λ, x_2) space. The shaded regions in all plots represent the standard deviations of the estimations performed over multiple trajectories and the solid lines represent the mean of the corresponding estimations. The green line in each plot represents the threshold value of mutual information between pairs of dynamical variables above which the value of mutual information can be considered as "significant." It is obtained by calculating mutual information from the randomly shuffled trajectories.

described in Eq. (2). Moreover, in our system, it is physically impossible for information to flow from any of the particles to the external drive since the drive is independent of them. As a result, the information pathways in the presence of hydrodynamic interaction can be diagrammatically represented as $\lambda \longrightarrow x_1 \rightleftarrows x_2$ for moderate nonequilibrium strengths (such as $\theta = 0.56$). However, if the nonequilibrium strength is increased such that $\theta \gg 1$ (which is beyond our experimental regime), the information pathways for our system will be fully unidirectional as $\lambda \longrightarrow x_1 \longrightarrow x_2$. We further demonstrate this with numerical evidence in Fig. 6 in Appendix D. Note that we present estimates of time-delayed mutual information using a kNN estimator in a fully data-driven manner. For this system, however, the same quantity can also be calculated analytically in terms of the two-point correlation function, since the dynamics are Gaussian. Consequently, the time lag at which the global maximum occurs for the time-delayed mutual information between any two variables corresponds to the time of maximum correlation or anticorrelation, e.g., $\langle x(t)y(t+\tau)\rangle$. The time-dependent cross-correlation functions between different dynamical variables are displayed in Fig. 8 in Appendix E. As further shown in Appendix F, the analytical estimates of time-delayed mutual information reasonably match the numerical estimates. All in all, this informational pathway is indeed a signature of *hierarchical* interaction as the presence of the external active drive λ is partially available to the fixed particle x_2 through the hydrodynamic interaction.

To establish this causal directionality further, we next estimate *transfer entropy* [as defined in Eq. (3)], which is capable of capturing only the exchanged information between two subsystems by excluding the history of the target. To compute the transfer entropy from the experimental and numerical trajectories, we used the recently proposed Markov state model–based estimation technique because of its simplicity and calculation efficiency [28,73].

Similarly to time-delayed mutual information, $TE_{\lambda\to x_1}(\tau)$, $TE_{x_1\to x_2}(\tau)$, and $TE_{\lambda\to x_2}(\tau)$ also possess global maxima at different time lags (shown in Fig. 4), and $TE_{\lambda\to x_1}(\tau) \gg TE_{x_1\to\lambda}(\tau)$ and $TE_{\lambda\to x_2}(\tau) \gg TE_{x_2\to\lambda}(\tau)$. Additionally, a global maximum is indeed present in $TE_{x_2\to x_1}(\tau)$. The particular time lag at which the global maximum occurs for the transfer entropy between any two dynamical variables corresponds to the time of maximum correlation or anticorrelation between those two variables as well. Moreover, the appearance of two peaks in $TE_{\lambda\to x_2}(\tau)$ is also related to the nonintuitive behavior of $\langle\lambda(t)x_2(t+\tau)\rangle$—which possesses two local extrema at two different time lags. It is worth noting that while

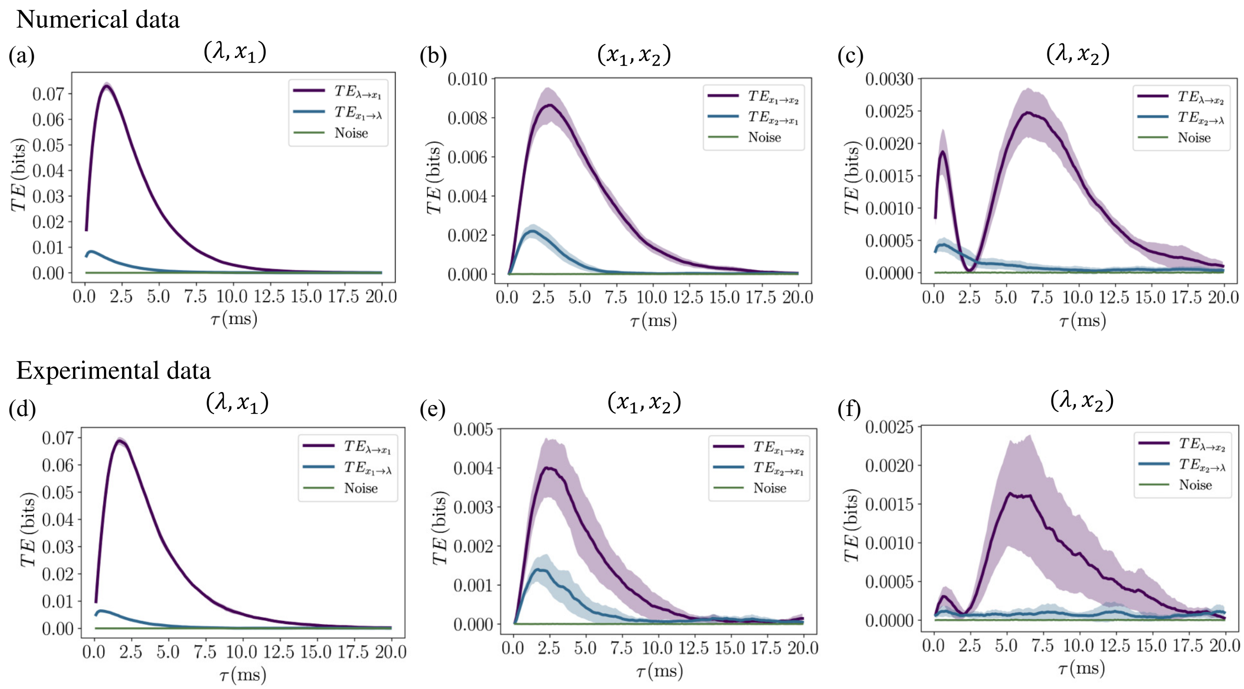

FIG. 4. Estimated transfer entropies between different dynamic variables of the system with $\theta = 0.56$ and $\epsilon = 0.49$ in (a),(d) (λ, x_1) space, (b),(e) (x_1, x_2) space, and (c),(f) (λ, x_2) space. The shaded regions in all plots represent the standard deviations of the estimations performed over multiple trajectories and the solid lines represent the mean of the corresponding estimations. The green line in each plot represents the threshold value of transfer entropy between pairs of dynamical variables above which the value of transfer entropy can be considered as "significant." It is obtained by calculating transfer entropy from the randomly shuffled trajectories.

the time-dependent cross-correlation function quantifies linear correlations between the dynamic variables, the time-delayed mutual information and the transfer entropy are capable of capturing both linear and nonlinear dependencies between different variables of a generic system, thereby revealing richer dynamical structure [25].

The overall features of transfer entropies between different dynamical variables indicate a unique direction of information flow that matches with the direction suggested by the characteristics of the time-delayed mutual information. Moreover, it can be further ascertained that in a moderate nonequilibrium scenario, the information pathways between hydrodynamically coupled particles are bidirectional, and can be made completely unidirectional by increasing the strength of the nonequilibrium drive. Moreover, the asymmetry of the time-delayed quantities also depends on ϵ for a given θ—as shown in Fig. 7 in Appendix D—with the time-delayed information measures estimated for $\theta = 0.56$ and $\epsilon = 0.29$.

To further explore such dependencies on the system parameters, we introduce a measure of asymmetry in causal directionality for any generic (x, y) phase space, defined as the difference in magnitudes of the transfer entropies estimated at the lag time corresponding to the maximum information transfer of $TE_{x\to y}$, i.e., $\mathcal{A}_{x\to y}(\tau^{\max}_{x\to y}) = TE_{x\to y}(\tau^{\max}_{x\to y}) - TE_{y\to x}(\tau^{\max}_{x\to y})$. We then compute this parameter for all bivariate subspaces of our system using numerical trajectories generated by varying θ (fixed τ_e) and ϵ. The results are shown in Fig. 5. We find that the asymmetry parameter strongly depends on these two parameters and the choice of the subspace. The asymmetry is slightly lowered for (λ, x_1) space as ϵ is increased for a fixed θ [Fig. 5(a)]. In contrast, this dependency is reversed in both (x_1, x_2) space [Fig. 5(b)] and (λ, x_2) space [Fig. 5(c)], where the asymmetry is higher with higher ϵ for any fixed θ. Such features of asymmetry suggest that while higher ϵ induces nonequilibrium character in (x_1, x_2) space and (λ, x_2) space, it reduces the same in (λ, x_1) space. This is consistent with our observation regarding the dependence of pairwise mutual information between different variables, and further substantiates the counterintuitive role of hydrodynamic interaction in shaping the irreversibility of the process in different subspaces. Moreover, the theoretically estimated partial entropy production rates in these (coarse-grained) subspaces also exhibit similar signatures as a function of θ and ϵ, as shown in Fig. 10 in Appendix G.

Note that, in contrast, at the equilibrium limit (in the absence of external driving), both time-delayed information measures possess a symmetric feature (shown

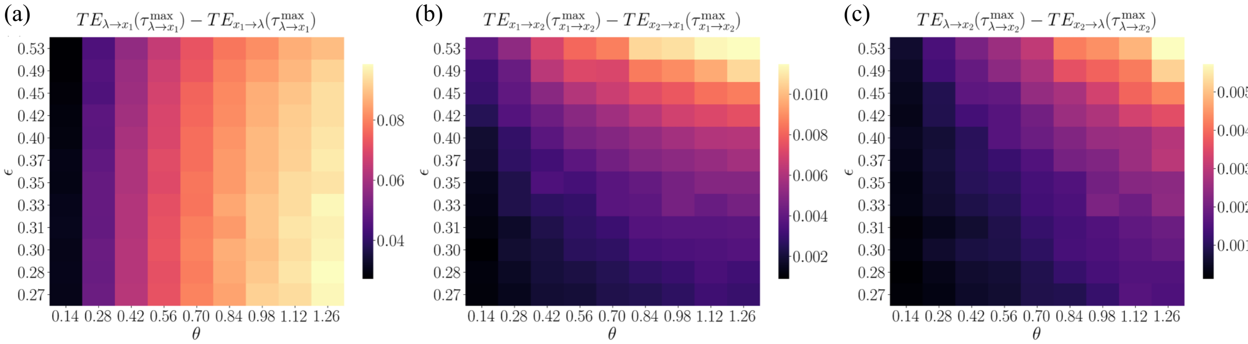

FIG. 5. Asymmetry of transfer entropies as a function of θ and ϵ, estimated at the lag time corresponding to the maximum information transfer in (a) (λ, x_1) space, (b) (x_1, x_2) space, and (λ, x_2) space. The values represent the mean of ten independent estimations, each based on distinct numerical trajectories, for every pair of θ and ϵ.

in Fig. 11 in Appendix H) such that $MI_{x_1\to x_2}(\tau) \sim MI_{x_2\to x_1}(\tau)$ and $TE_{x_1\to x_2}(\tau) \sim TE_{x_2\to x_1}(\tau)$, which indicates a strong bidirectional $\left(x_1 \rightleftarrows x_2 \right)$ nature of information flow between the particles. Indeed, this is consistent with the fact that dynamic correlations in equilibrium configurations are usually symmetric, i.e., $\langle x(t)y(t+\tau)\rangle = \langle y(t)x(t+\tau)\rangle$ [38].

V. CONCLUSIONS

In conclusion, we use information-theoretic techniques to explore the role of hydrodynamic interactions in establishing mutual dependencies between various degrees of freedom in the presence of an *active* drive. Our analysis reveals that while such interactions promote informational exchange between the coupled particles, the mutual information between the external drive and the driven particle, gets slightly reduced. This explains a previously observed counterintuitive dependence of the irreversibility of this system on the strength of interactions [48], especially under coarse-graining. Moreover, the emergent causal structure in every phase plane of the system—estimated through the time-delayed information-theoretic measures—quantifies the crucial role of the nonequilibrium drive in manifesting directional influence between the particles. These findings further underscore the effectiveness of information-theoretic measures in uncovering the nonequilibrium origin in a complex system or their ability to distinguish nonequilibrium processes from their equilibrium counterparts. While our study focuses on a particular type of pairwise interactions, the analysis we presented here can be further generalized to nonequilibrium systems with multiple interacting degrees of freedom, under different kinds [3,74–76] and higher orders [4,58,77] of interaction.

Such detailed knowledge of the role of interaction could be especially informative for manipulating the kinetics of mesoscopic systems subjected to nonequilibrium environments with unprecedented control and precision [78,79]. Reciprocally, analyses of the flow of information at various levels can also be used to elicit detailed information about the kinetics of molecular machines that function in highly nonequilibrium environments [80]. Another relevant problem of interest could be the control of microsystems comprising multiple particles with targeted features in a fluidic environment—where hydrodynamic interaction is prevalent [68,81–83]. Additionally, the prospect of achieving dynamical information synergy [69] in these systems through hydrodynamic interactions by harnessing such information flow structures can also be explored. We will investigate some of these aspects in future work.

ACKNOWLEDGMENTS

The work was supported by IISER Kolkata and the Science and Engineering Research Board, Department of Science and Technology, Government of India, through Grant No. CRG/2022/002417. B.D. is thankful to the Ministry of Education of the Government of India for financial support through a Prime Minister's Research Fellowship grant. S.K.M. acknowledges the Knut and Alice Wallenberg Foundation for financial support through Grant No. KAW 2021.0328.

DATA AVAILABILITY

The data that support the findings of this article are not publicly available. The data are available from the authors upon reasonable request.

APPENDIX A: COVARIANCE MATRIX

The elements of the covariance matrix **C** of the steady-state distribution of the whole system can be estimated as follows:

$$
\begin{aligned}
c_{x_1x_1} &= \frac{D_0\tau_1\left(-\tau_2^2\left(\alpha^2\theta+\alpha+1\right)+\alpha\tau_1^2\left(\alpha\left(\epsilon^2-1\right)(\alpha\theta+1)-1\right)+\tau_2\tau_1\left(\alpha\left(\alpha\left(\epsilon^2-1\right)(\alpha\theta+\theta+1)-2\right)-1\right)\right)}{(\tau_1+\tau_2)\left(\alpha\tau_1\left(\alpha\left(\epsilon^2-1\right)-1\right)-(\alpha+1)\tau_2\right)},\\
c_{x_1x_2} &= c_{x_2x_1} = -\frac{\alpha^2 D_0\theta\tau_1\tau_2^2\epsilon}{(\tau_1+\tau_2)\left(\alpha\tau_1\left(\alpha\left(\epsilon^2-1\right)-1\right)-(\alpha+1)\tau_2\right)},\\
c_{x_1\lambda} &= c_{\lambda x_1} = \frac{\alpha^2 D_0\theta\tau_1\left(\alpha\tau_1\left(\epsilon^2-1\right)-\tau_2\right)}{\alpha\tau_1\left(\alpha\left(\epsilon^2-1\right)-1\right)-(\alpha+1)\tau_2},\\
c_{x_2x_2} &= -\frac{D_0\tau_2\left((\alpha+1)\tau_2^2+\tau_2\tau_1\left(\alpha\left(\alpha(\theta-1)\epsilon^2+\alpha+2\right)+1\right)+\alpha\tau_1^2\left(-\alpha\epsilon^2+\alpha+1\right)\right)}{(\tau_1+\tau_2)\left(\alpha\tau_1\left(\alpha\left(\epsilon^2-1\right)-1\right)-(\alpha+1)\tau_2\right)},\\
c_{x_2\lambda} &= c_{\lambda x_2} = -\frac{\alpha^2 D_0\theta\tau_1\tau_2\epsilon}{\alpha\tau_1\left(\alpha\left(\epsilon^2-1\right)-1\right)-(\alpha+1)\tau_2},\\
c_{\lambda\lambda} &= \alpha D_0\theta\tau_1.
\end{aligned}
\tag{A1}
$$

APPENDIX B: MUTUAL INFORMATION

The pairwise mutual information between the external drive and the driven particle can be estimated with use of the corresponding submatrices of the steady-state covariance matrix [according to Eq. (7)] as

$$
MI_{\lambda x_1} = \frac{1}{2}\log_2\left(\frac{\mathcal{P}}{\mathcal{Q}}\right), \tag{B1}
$$

where

$$
\begin{aligned}
\mathcal{P} &= \left(\alpha\tau_1\left(\alpha\left(\epsilon^2-1\right)-1\right)-(\alpha+1)\tau_2\right)\left(-\tau_2^2\left(\alpha^2\theta+\alpha+1\right)+\alpha\tau_1^2\left(\alpha\left(\epsilon^2-1\right)(\alpha\theta+1)-1\right)\right.\\
&\quad\left.+\tau_2\tau_1\left(\alpha\left(\alpha\left(\epsilon^2-1\right)(\alpha\theta+\theta+1)-2\right)-1\right)\right),\\
\mathcal{Q} &= \alpha^2\tau_1^3\left(\alpha\left(\epsilon^2-1\right)\left(\alpha\left(-\theta+\epsilon^2-1\right)-2\right)+1\right)\\
&\quad+\tau_2^3(\alpha(\alpha\theta+\alpha+2)+1)+\alpha\tau_2\tau_1^2\left(\alpha\left(\alpha\left(\epsilon^2-1\right)\left(\alpha(\theta+1)\left(\epsilon^2-1\right)-2(\theta+2)\right)\right.\right.\\
&\quad\left.\left.-2\epsilon^2+5\right)+2\right)+\tau_2^2\tau_1\left(\alpha\left(\alpha\left(-2\alpha(\theta+1)\left(\epsilon^2-1\right)+\theta-\left((\theta+2)\epsilon^2\right)+5\right)+4\right)+1\right).
\end{aligned}
\tag{B2}
$$

$MI_{\lambda x_1}$ in the absence of the second particle reduces to

$$
MI_{\lambda x_1}|_{\epsilon\to 0} = \frac{1}{2}\log_2\left(\frac{(\alpha+1)\left(\alpha^2\theta+\alpha+1\right)}{\alpha(\alpha\theta+\alpha+2)+1}\right), \tag{B3}
$$

which is evidently larger than $MI_{\lambda x_1}$.

Similarly, the mutual information between the particles can be computed [according to Eq. (6)] as

$$
MI_{x_1x_2} = \frac{1}{2}\log_2\left(\frac{\mathcal{R}}{\mathcal{S}}\right), \tag{B4}
$$

where

$$
\begin{aligned}
\mathcal{R} &= \left(-(\alpha+1)\tau_2^2-\tau_2\tau_1\left(\alpha\left(\alpha(\theta-1)\epsilon^2+\alpha+2\right)+1\right)+\alpha\tau_1^2\left(\alpha\left(\epsilon^2-1\right)-1\right)\right)\\
&\quad\times\left(-\tau_2^2\left(\alpha^2\theta+\alpha+1\right)+\alpha\tau_1^2\left(\alpha\left(\epsilon^2-1\right)(\alpha\theta+1)-1\right)+\tau_2\tau_1\left(\alpha\left(\alpha\left(\epsilon^2-1\right)(\alpha\theta+\theta+1)-2\right)-1\right)\right),\\
\mathcal{S} &= \alpha^2\tau_1^4\left(\alpha\left(\epsilon^2-1\right)-1\right)\left(\alpha\left(\epsilon^2-1\right)(\alpha\theta+1)-1\right)+\alpha\tau_1^3\tau_2\left(\alpha\left(\alpha\left(-\left(\alpha^2\theta\left(\epsilon^2-1\right)\left((\theta-2)\epsilon^2+2\right)\right)\right.\right.\right.\\
&\quad+\ 2\alpha\left(\epsilon^2-1\right)\left(-2\theta+\epsilon^2-1\right)+2(\theta+3)-(\theta+6)\epsilon^2\Big)-2\epsilon^2+6\Big)+2\Big)\\
&\quad+\Big(\alpha\Big(\alpha\Big(\alpha\Big(-\left(\alpha^2\theta\left(\epsilon^2-1\right)\left((\theta-1)\epsilon^2+1\right)\right)
\end{aligned}
$$

$$- \alpha\left(\epsilon^2-1\right)\left(5\theta+\left(\theta^2-1\right)\epsilon^2+1\right)+5\theta-2(\theta+3)\epsilon^2+6\Big)+\theta-4\epsilon^2+10\Big)+6\Big)+1\Big)\times\tau_1^2\tau_2^2$$
$$+(\alpha+1)\tau_2^4\left(\alpha^2\theta+\alpha+1\right)+\tau_1\tau_2^3\left(\alpha\left(\alpha\left(\alpha\left(2(\alpha+2)\theta-\left(\epsilon^2(2\alpha\theta+\theta+2)\right)+2\right)+2\theta-2\epsilon^2+6\right)+6\right)+2\right). \tag{B5}$$

Note that if the particles are well separated such that $\epsilon \to 0$, $MI_{x_1x_2}$ also vanishes. Furthermore, the dependence between the fixed particle x_2 and the external drive λ can also be estimated through their mutual information as

$$MI_{\lambda x_2} = \frac{1}{2}\log_2\frac{c_{\lambda\lambda}c_{x_2x_2}}{\det \mathbf{C}_{\lambda x_2}} = \frac{1}{2}\log_2\left(\frac{\mathcal{T}}{\mathcal{U}}\right), \tag{B6}$$

where

$$\mathcal{T} = \left(\alpha\tau_1\left(\alpha\left(\epsilon^2-1\right)-1\right)-(\alpha+1)\tau_2\right)\left(-(\alpha+1)\tau_2^2-\tau_2\tau_1\left(\alpha\left(\alpha(\theta-1)\epsilon^2+\alpha+2\right)+1\right)+\alpha\tau_1^2\left(\alpha\left(\epsilon^2-1\right)-1\right)\right),$$
$$\mathcal{U} = \alpha^2\tau_1^3\left(-\alpha\epsilon^2+\alpha+1\right)^2+(\alpha+1)^2\tau_2^3+\alpha\tau_2\tau_1^2\left(\alpha\left(-\alpha\left(\epsilon^2-1\right)\left(\alpha(\theta-1)\epsilon^2+\alpha+4\right)-2\epsilon^2+5\right)+2\right)$$
$$+\tau_2^2\tau_1\left(\alpha\left(\alpha\left(-2\alpha\left(\epsilon^2-1\right)+(\theta-2)\epsilon^2+5\right)+4\right)+1\right). \tag{B7}$$

Importantly, $MI_{\lambda x_2} \neq 0$ as long as $\epsilon \neq 0$, and $MI_{\lambda x_2} < MI_{\lambda x_1}$, which indicates that the external driving is partially available to the fixed particle via hydrodynamic interaction.

APPENDIX C: DETAILS OF NUMERICAL SIMULATION OF THE EXPERIMENTAL SYSTEM

The coupled *Langevin* equations that describe the dynamics of our system are provided in Eq. (4). Noticeably, the diffusion matrix $\mathbf{D}$ for this system is not diagonal due to its connection with the hydrodynamic coupling tensor, so the matrix incorporating the strength of the appropriate noise terms ($\mathbf{G}$) is calculated after Cholesky decomposition has been performed such that $\mathbf{D} = \frac{1}{2}\mathbf{G}\mathbf{G}^T$ [48]. The noise matrix $\mathbf{G}$ of our system takes the form

$$\mathbf{G} = \begin{pmatrix} \sqrt{2D_0} & 0 & 0 \\ \epsilon\sqrt{2D_0} & \sqrt{2(D_0-\epsilon^2 D_0)} & 0 \\ 0 & 0 & \sqrt{2\theta D_0} \end{pmatrix}. \tag{C1}$$

Then the linear, stochastic differential equations with the drift [Eq. (5)] and noise matrices are numerically discretized with fixed time step $\Delta t = 1\times 10^{-4}$ s (which is less than all timescales present in the systems), and the first-order Eurler-Maruyama method is used to perform the integration. The discretized forms of the dynamical equations are

$$\begin{aligned} x_1^{t+\Delta t} &= x_1^t - (1/\tau_1)\,x_1^t\Delta t - (\epsilon/\tau_2)x_2^t\Delta t + (1/\tau_1)\,\lambda^t\Delta t + \sqrt{2D_0\Delta t}\,\eta_1^t, \\ x_2^{t+\Delta t} &= x_2^t - (\epsilon/\tau_1)\,x_1^t\Delta t - (1/\tau_2)x_2^t\Delta t + (\epsilon/\tau_1)\,\lambda^t\Delta t + \epsilon\sqrt{2D_0\Delta t}\eta_1^t + \sqrt{2(D_0-\epsilon^2 D_0)\Delta t}\,\eta_2^t, \\ \lambda^{t+\Delta t} &= \lambda^t - (1/(\alpha\tau_1))\lambda^t\Delta t + \sqrt{2\theta D_0\Delta t}\eta_3^t, \end{aligned} \tag{C2}$$

where $\eta_i^t \sim \mathcal{N}(0,1)$ is sampled from a Gaussian distribution with zero mean and unit variance, and the initial states $(x_1^0, x_2^0, \lambda^0)$ of the individual degrees of freedom are sampled from normal distributions with zero mean and appropriate variances such that $x_1^0 \sim \mathcal{N}(0,\sigma_1^2)$, $x_2^0 \sim \mathcal{N}(0,\sigma_2^2)$, and $\lambda^0 \sim \mathcal{N}(0,\sigma_\lambda^2)$, with $\sigma_1 = \sqrt{k_BT/k_1}$, $\sigma_2 = \sqrt{k_BT/k_2}$, and $\sigma_\lambda = \sqrt{D_e/\tau_e}$. The system parameters (τ_1, τ_2, τ_e, D_0, and α) remain the same as mentioned in Sec. III for every numerical simulation.

APPENDIX D: TIME-DELAYED INFORMATION MEASURES FOR OTHER VALUES OF θ and ϵ

We estimate the time-delayed mutual information and the transfer entropy for the system with higher nonequilibrium strength $\theta = 5.6$ from numerical trajectories. As we show in Fig. 6, the unidirectionality of information flow in the hierarchical dynamics for higher activity strength can be observed from the pronounced asymmetry of transfer entropy estimated between different variables

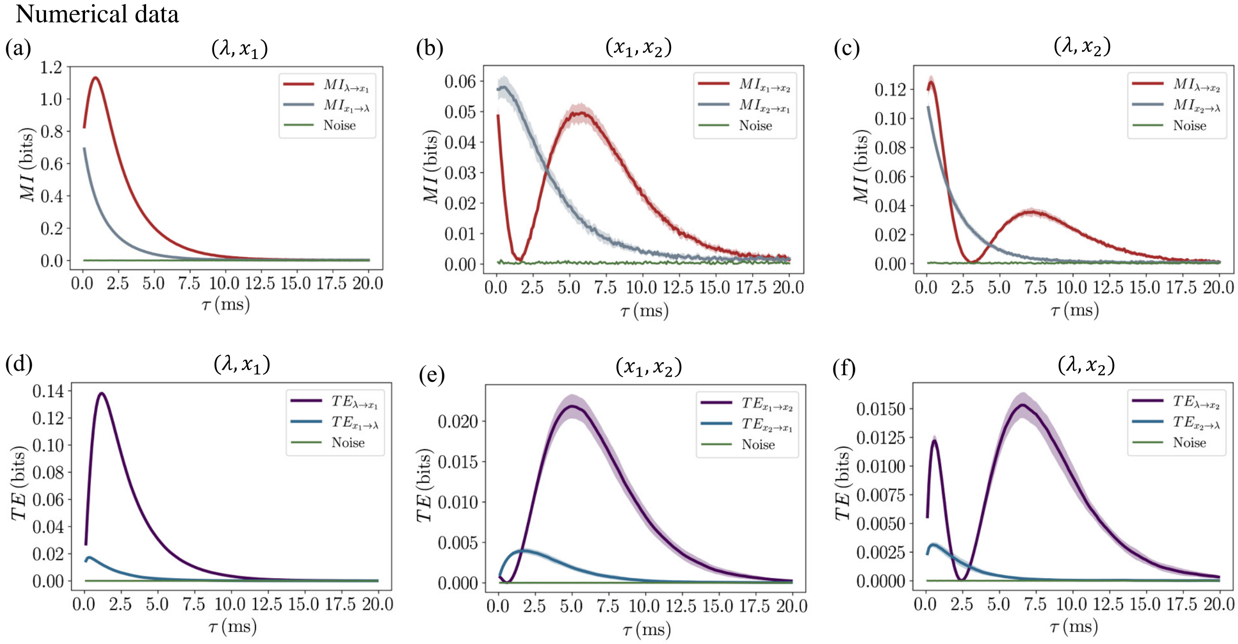

FIG. 6. Estimation of time-delayed information measures for the system with $\theta = 5.6$ and $\epsilon = 0.49$: (a)–(c) time-delayed mutual information; (d)–(f) transfer entropies between different variables estimated in (a),(d) (λ, x_1) space, (b),(e) (x_1, x_2) space, and (c),(f) (λ, x_2) space.

of the system as $TE_{\lambda\to x_1} \gg TE_{x_1\to\lambda}$, $TE_{x_1\to x_2} \gg TE_{x_2\to x_1}$, and $TE_{\lambda\to x_2} \gg TE_{x_2\to\lambda}$. Additionally, the magnitude of time-delayed measures also depends on the interaction strength ϵ, while the strength of the external drive θ is fixed. As displayed in Fig. 7, the peak magnitude of $TE_{\lambda\to x_1}$ is slightly higher than the same for $\epsilon = 0.49$ (Fig. 4), while the peak magnitudes of $TE_{x_1\to x_2}$ and $TE_{\lambda\to x_2}$ are reduced compared with the values for $\epsilon = 0.49$ (Fig. 4).

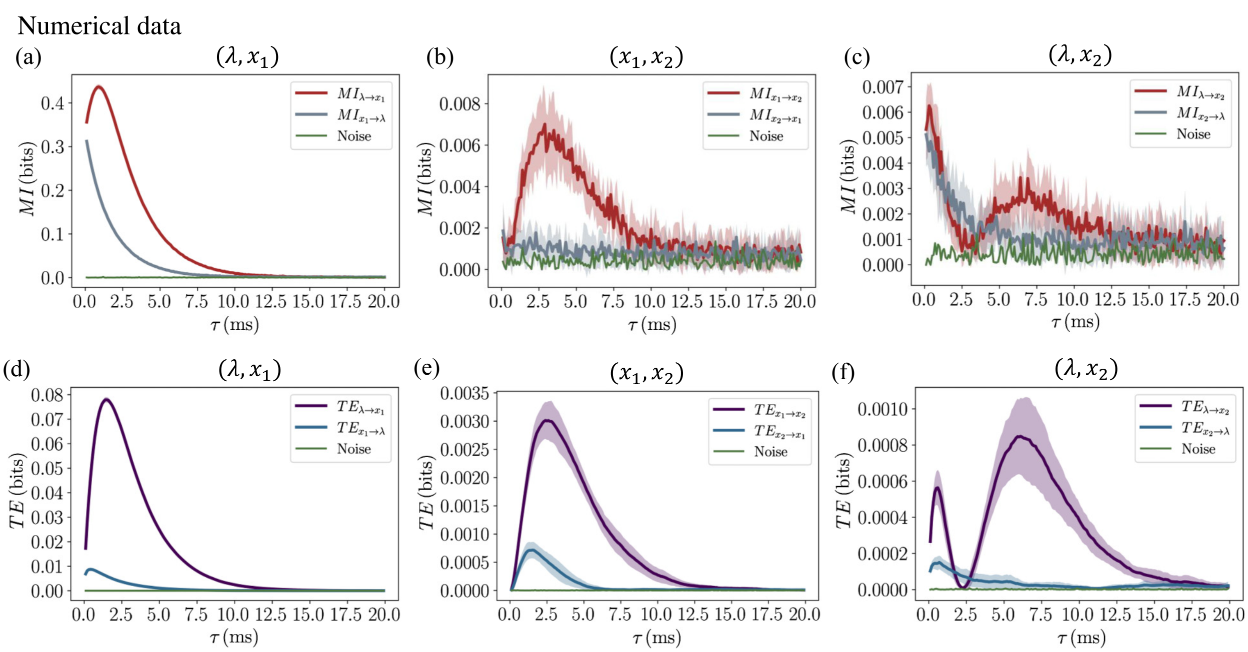

FIG. 7. Estimation of time-delayed information measures for the system with $\theta = 0.56$ and $\epsilon = 0.29$: (a)–(c) time-delayed mutual information; (d)–(f) transfer entropy between different variables estimated in (a),(d) (λ, x_1) space, (b),(e) (x_1, x_2) space, and (c),(f) (λ, x_2) space.

The same can be further understood from the inhomogeneous features of asymmetry parameters as a function of θ and ϵ in every bivariate subspace of our system, as shown in Fig. 5.

APPENDIX E: TIME-DEPENDENT CROSS-CORRELATION FUNCTIONS

The two-time correlation matrix $\langle \mathbf{x}(t)\mathbf{x}(t+\tau)\rangle$ corresponding to the system as a function of time lag $\tau(>0)$ can be calculated as [68,84]

$$\mathbf{C}_{\mathbf{xx}}(\tau) \equiv \langle \mathbf{x}(t)\mathbf{x}(t+\tau)\rangle = [\exp[-\mathbf{F}\tau]\mathbf{C}]^T. \quad \text{(E1)}$$

Furthermore, each two-time cross-correlation function can be normalized, e.g., $NC_{x_1x_2}(\tau) = \langle x_1(t)x_2(t+\tau)\rangle/\sqrt{\text{var}(x_1)}\sqrt{\text{var}(x_2)} \equiv \langle x_1(t)x_2(t+\tau)\rangle/\sqrt{c_{x_1x_1}}\sqrt{c_{x_2x_2}}$, $NC_{\lambda x_1}(\tau) = \langle \lambda(t)x_1(t+\tau)\rangle/\sqrt{\text{var}(\lambda)}\sqrt{\text{var}(x_1)} \equiv \frac{\langle \lambda(t)x_1(t+\tau)\rangle}{\sqrt{c_{\lambda\lambda}}\sqrt{c_{x_1x_1}}}$, $NC_{\lambda x_2}(\tau) = \langle \lambda(t)x_2(t+\tau)\rangle/\sqrt{\text{var}(\lambda)}\sqrt{\text{var}(x_2)} \equiv \langle \lambda(t)x_2(t+\tau)\rangle/\sqrt{c_{\lambda\lambda}}\sqrt{c_{x_2x_2}}$, and so on.

We do not provide detailed analytical expressions for each correlation function for brevity. However, we plot the normalized cross-correlation functions corresponding to the dynamical variables in Fig. 8 for a particular set of fixed parameters: $D_0 \sim 0.16\ \mu\text{m}^2/s$, $\tau_1 \sim 1.5$ ms, $\tau_2 \sim 2.1$ ms, and $\alpha \sim 2.7$. It is quite evident that the two-time correlation functions corresponding to any two dynamical variables are asymmetric in the presence of nonequilibrium drive as $NC_{\lambda x_1}(\tau) \neq NC_{x_1\lambda}(\tau)$, $NC_{x_1x_2}(\tau) \neq NC_{x_2x_1}(\tau)$, and $NC_{\lambda x_2}(\tau) \neq NC_{x_2\lambda}(\tau)$. These asymmetric features are enhanced with the increase in nonequilibrium strength [85]. In this context, the dynamics of the driven particle $x_1(t)$ are positively correlated with the external nonequilibrium drive $\lambda(t)$, and $NC_{\lambda x_1}(\tau)$ possesses a global maxima at a particular delay time [Figs. 8(a) and 8(d)]. On the other hand, the trapped particles are anticorrelated and the corresponding (anti)correlations [$NC_{x_1x_2}(\tau)$ and $NC_{x_2x_1}(\tau)$] also peak at a particular time lag [Figs. 8(b) and 8(e)]. A discussed in the main text, the corresponding time-delayed information-theoretic quantities (time-delayed mutual information and transfer entropy) also display global maxima at these particular time lags. Moreover, the correlation function between the external drive and the fixed particle, $NC^{\tau}_{\lambda x_2}$, shows both maximum positive correlation and maximum negative correlation at two different time lags [Figs. 8(c) and 8(f)]. As a result, both time-delayed mutual information $MI_{\lambda\to x_2}(\tau)$ and transfer entropy $TE_{\lambda\to x_2}(\tau)$ between these two variables also show two peaks at two different time lags.

APPENDIX F: ANALYTICAL ESTIMATION OF TIME-DELAYED MUTUAL INFORMATION

For a stochastic system with a multivariate Gaussian distribution, the time-delayed mutual information between different degrees of freedom can be estimated analytically as well. For any two such variables x and y—whose joint distribution is bivariate Gaussian—the time-delayed mutual information $MI_{x\to y}(\tau)$ defined in Eq. (2) can be

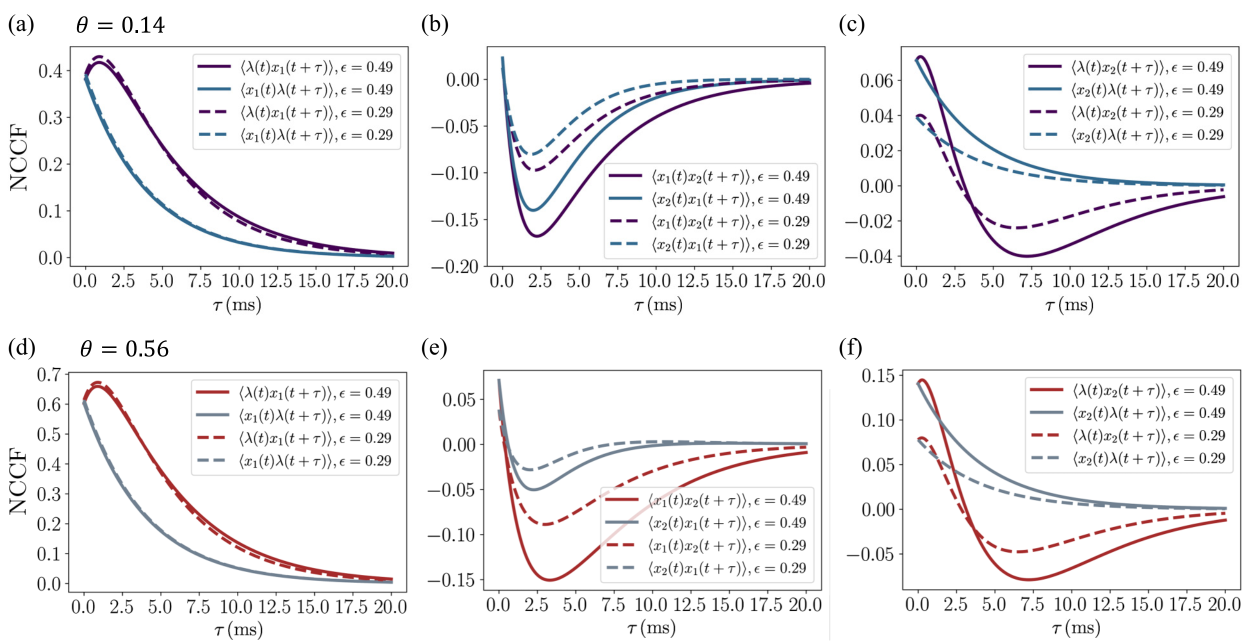

FIG. 8. Analytically estimated normalized cross-correlation function (NCCF) corresponding to the dynamical variables for two different noise strengths θ: (a)–(c) $\theta = 0.14$; (d)–(f) $\theta = 0.56$.

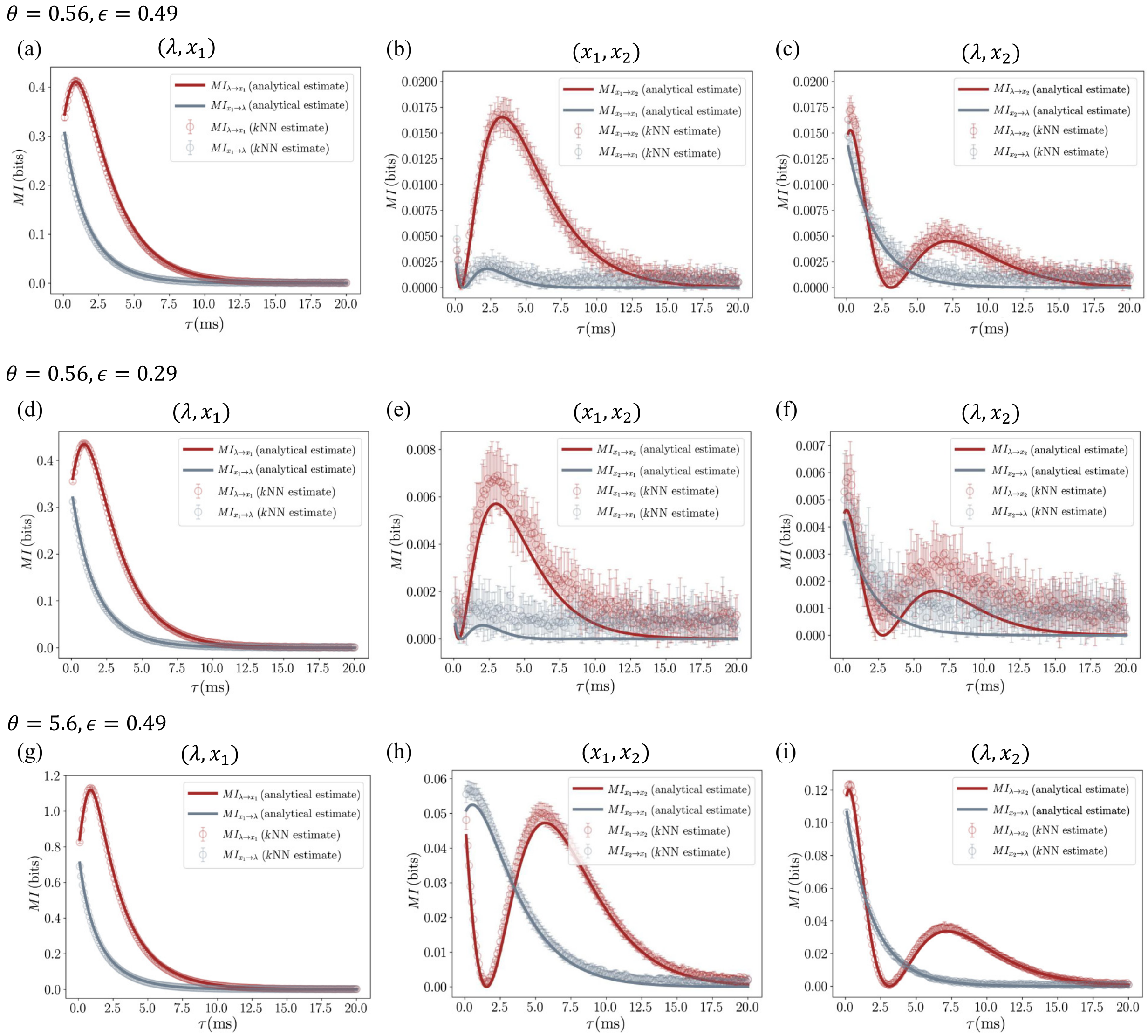

FIG. 9. Analytically estimated time-delayed mutual information in different bivariate planes, along with the corresponding kNN estimates, for different values of θ and ϵ.

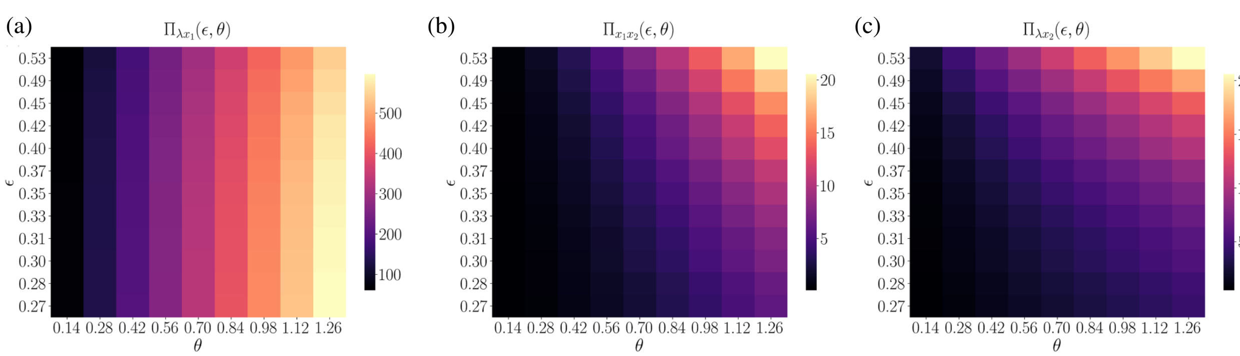

FIG. 10. Theoretically estimated partial entropy production rates (in the unit of k_B/s) as a function of θ and ϵ for (a) (λ, x_1) space, (b) (x_1, x_2) space, and (λ, x_2) space.

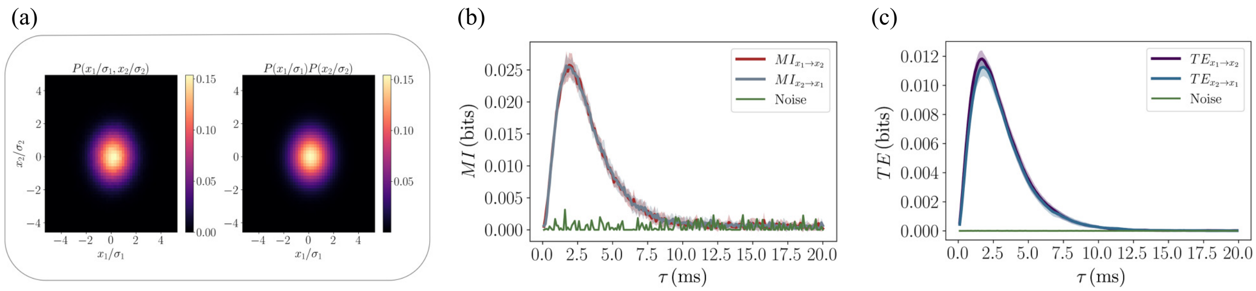

FIG. 11. (a) Joint probability distribution of the displacements of the particles at the equilibrium steady state can be exactly factorized as the product of the marginals. (b) Time-delayed mutual information and (c) transfer entropy between the particles [(x_1, x_2) space] with hydrodynamic interaction $\epsilon = 0.49$ estimated from the numerical trajectories of the system without a nonequilibrium drive. The green line in each plot denotes the estimates from the randomly shuffled trajectories.

analytically rewritten as

$$MI_{x\to y}(\tau) \equiv I(x_t; y_{t+\tau}) = \frac{1}{2}\log_2 \frac{c_{xx}c_{yy}}{\det \mathbf{C}_{xy}(\tau)}, \tag{F1}$$

following its time-independent counterpart. Here $\mathbf{C}_{xy}(\tau)$ is the time-delayed covariance matrix defined as

$$\mathbf{C}_{xy}(\tau) = \begin{pmatrix} \langle x_t x_t\rangle & \langle x_t y_{t+\tau}\rangle \\ \langle y_{t+\tau}x_t\rangle & \langle y_{t+\tau}y_{t+\tau}\rangle \end{pmatrix} = \begin{pmatrix} c_{xx} & c_{xy}(\tau) \\ c_{xy}(\tau) & c_{yy} \end{pmatrix}. \tag{F2}$$

Hence, $MI_{x\to y}(\tau)$ can be analytically represented through the elements of $\mathbf{C}_{xy}(\tau)$ as

$$MI_{x\to y}(\tau) = \frac{1}{2}\log_2 \frac{c_{xx}c_{yy}}{c_{xx}c_{yy} - c_{xy}(\tau)^2}. \tag{F3}$$

It is now clear that if $c_{xy}(\tau) \neq c_{yx}(\tau)$, $MI_{x\to y}(\tau) \neq MI_{y\to x}(\tau)$—suggesting a preferred directionality of information flow. Following this, we can analytically estimate $MI_{\lambda\to x_1}(\tau)$, $MI_{x_1\to x_2}(\tau)$, and $MI_{\lambda\to x_2}(\tau)$ along with their reverse counterparts using the elements of the covariance matrix [as given in Eqs. (A1)] and the elements of the two-time correlation matrix [Eq. (E1)]. As shown in Fig. 9, the numerically computed time-delayed mutual information reasonably matches with the corresponding analytical estimations. This further suggests that the particular time lags at which maxima occur for the time-delayed mutual information are indeed related to the time lag of extremum two-point (anti)correlation.

APPENDIX G: PARTIAL ENTROPY PRODUCTION RATE AT BIVARIATE PLANES

The partial entropy production rate for each bivariate phase plane of this system can be estimated analytically with use of the method described in Ref. [50]. While we demonstrated this explicitly for the (x_1, x_2) phase plane in Ref. [48], the same analysis can be extended to other phase planes as well. The partial entropy production rates corresponding to all bivariate planes (coarse-grained subspaces) of our system are illustrated in Fig. 10. The features of such partial or reduced entropy production rates in each plane show a similar dependence on ϵ and θ as that observed in the asymmetry of transfer entropies in the corresponding phase planes (Fig. 5). This further highlights the intricate connection between irreversibility and the asymmetry of transfer entropies.

APPENDIX H: COMPARISON WITH THE EQUILIBRIUM SCENARIO

In the absence of any external drive, the hydrodynamically coupled system will reach an equilibrium steady state in which the particles are statistically independent. Since the steady-state joint distribution of the displacement of the particles is exactly factorized as the product of marginals, i.e., $P(x_1, x_2) = P(x_1)P(x_2)$ [as shown in Fig. 11(a)], mutual information at the equilibrium steady state will be zero. The time-delayed information measures possess a symmetric feature such that $MI_{x_1\to x_2}(\tau) \sim MI_{x_2\to x_1}(\tau)$ [Fig. 11(b)] and $TE_{x_1\to x_2}(\tau) \sim TE_{x_2\to x_1}(\tau)$ [Fig. 11(c)], which indicates a strong bidirectional $(x_1 \rightleftarrows x_2)$ nature of information flow for the equilibrium configuration. The characteristics of the information flow in an equilibrium scenario are quite different from the same in a nonequilibrium configuration and are consistent with the fact that dynamic correlations in equilibrium configurations are usually symmetric, i.e., $\langle x(t)y(t+\tau)\rangle = \langle y(t)x(t+\tau)\rangle$.

[1] S. Bo and A. Celani, Multiple-scale stochastic processes: Decimation, averaging and beyond, Phys. Rep. **670**, 1 (2017).
[2] D. M. Busiello, D. Gupta, and A. Maritan, Coarse-grained entropy production with multiple reservoirs: Unraveling the

role of time scales and detailed balance in biology-inspired systems, Phys. Rev. Res. **2**, 043257 (2020).
[3] S. A. Loos and S. H. Klapp, Irreversibility, heat and information flows induced by non-reciprocal interactions, New J. Phys. **22**, 123051 (2020).
[4] G. Nicoletti and D. M. Busiello, Information propagation in multilayer systems with higher-order interactions across timescales, Phys. Rev. X **14**, 021007 (2024).
[5] M. Fruchart, R. Hanai, P. B. Littlewood, and V. Vitelli, Non-reciprocal phase transitions, Nature **592**, 363 (2021).
[6] M. E. Cates and J. Tailleur, Motility-induced phase separation, Annu. Rev. Condens. Matter Phys. **6**, 219 (2015).
[7] W. Bialek, A. Cavagna, I. Giardina, T. Mora, E. Silvestri, M. Viale, and A. M. Walczak, Statistical mechanics for natural flocks of birds, Proc. Natl. Acad. Sci. **109**, 4786 (2012).
[8] G. Falasco, R. Rao, and M. Esposito, Information thermodynamics of Turing patterns, Phys. Rev. Lett. **121**, 108301 (2018).
[9] F. Brauns, J. Halatek, and E. Frey, Phase-space geometry of mass-conserving reaction-diffusion dynamics, Phys. Rev. X **10**, 041036 (2020).
[10] D. M. Busiello, S. Liang, F. Piazza, and P. De Los Rios, Dissipation-driven selection of states in non-equilibrium chemical networks, Commun. Chem. **4**, 16 (2021).
[11] S. Liang, P. De Los Rios, and D. M. Busiello, Thermodynamic bounds on symmetry breaking in linear and catalytic biochemical systems, Phys. Rev. Lett. **132**, 228402 (2024).
[12] A. Hilfinger and J. Paulsson, Separating intrinsic from extrinsic fluctuations in dynamic biological systems, Proc. Natl. Acad. Sci. **108**, 12167 (2011).
[13] L. S. Tsimring, Noise in biology, Rep. Progr. Phys. **77**, 026601 (2014).
[14] A. V. Chechkin, F. Seno, R. Metzler, and I. M. Sokolov, Brownian yet non-Gaussian diffusion: From superstatistics to subordination of diffusing diffusivities, Phys. Rev. X **7**, 021002 (2017).
[15] C. E. Shannon, A mathematical theory of communication, Bell Syst. Tech. J. **27**, 379 (1948).
[16] T. M. Cover and J. A. Thomas, *Elements of Information Theory* (John Wiley & Sons, New York, 2005).
[17] G. Nicoletti, Information and criticality in complex stochastic systems, ArXiv:2302.14583.
[18] G. Nicoletti and D. M. Busiello, Mutual information disentangles interactions from changing environments, Phys. Rev. Lett. **127**, 228301 (2021).
[19] G. Nicoletti and D. M. Busiello, Mutual information in changing environments: Nonlinear interactions, out-of-equilibrium systems, and continuously varying diffusivities, Phys. Rev. E **106**, 014153 (2022).
[20] G. Nicoletti and D. M. Busiello, Information interference driven by environmental activity, Phys. Rev. Res. **6**, 043275 (2024).
[21] J. J. Tyson, K. Chen, and B. Novak, Network dynamics and cell physiology, Nat. Rev. Mol. Cell Biol. **2**, 908 (2001).
[22] G. Tkačik, C. G. Callan Jr, and W. Bialek, Information flow and optimization in transcriptional regulation, Proc. Natl. Acad. Sci. **105**, 12265 (2008).
[23] J. A. Vastano and H. L. Swinney, Information transport in spatiotemporal systems, Phys. Rev. Lett. **60**, 1773 (1988).
[24] C. Kirst, M. Timme, and D. Battaglia, Dynamic information routing in complex networks, Nat. Commun. **7**, 11061 (2016).
[25] S. Li, Y. Xiao, D. Zhou, and D. Cai, Causal inference in nonlinear systems: Granger causality versus time-delayed mutual information, Phys. Rev. E **97**, 052216 (2018).
[26] T. Schreiber, Measuring information transfer, Phys. Rev. Lett. **85**, 461 (2000).
[27] A. Kaiser and T. Schreiber, Information transfer in continuous processes, Physica D **166**, 43 (2002).
[28] T. Hempel and S. A. Loos, A simple reconstruction method to infer nonreciprocal interactions and local driving in complex systems, ArXiv:2403.09243.
[29] A. D. Sánchez, J. M. López, and M. A. Rodriguez, Nonequilibrium phase transitions in directed small-world networks, Phys. Rev. Lett. **88**, 048701 (2002).
[30] A. Lozano-Durán and G. Arranz, Information-theoretic formulation of dynamical systems: causality, modeling, and control, Phys. Rev. Res. **4**, 023195 (2022).
[31] S. A. Loos, S. H. Klapp, and T. Martynec, Long-range order and directional defect propagation in the nonreciprocal *XY* model with vision cone interactions, Phys. Rev. Lett. **130**, 198301 (2023).
[32] S. Ito and T. Sagawa, Information thermodynamics on causal networks, Phys. Rev. Lett. **111**, 180603 (2013).
[33] S. Ito and T. Sagawa, Maxwell's demon in biochemical signal transduction with feedback loop, Nat. Commun. **6**, 7498 (2015).
[34] M. Samsuzzaman, M. Hasanuzzaman, A. Sayeed, and A. Saha, Flow of information in a mechanically quenched confined flock, Proc. Roy. Soc. A **481**, 20250063 (2025).
[35] T. Sagawa and M. Ueda, Role of mutual information in entropy production under information exchanges, New J. Phys. **15**, 125012 (2013).
[36] R. Chetrite, M. Rosinberg, T. Sagawa, and G. Tarjus, Information thermodynamics for interacting stochastic systems without bipartite structure, J. Stat. Mech.: Theory Exp. **2019**, 114002 (2019).
[37] R. E. Spinney, J. T. Lizier, and M. Prokopenko, Transfer entropy in physical systems and the arrow of time, Phys. Rev. E **94**, 022135 (2016).
[38] J.-C. Meiners and S. R. Quake, Direct measurement of hydrodynamic cross correlations between two particles in an external potential, Phys. Rev. Lett. **82**, 2211 (1999).
[39] C. Maggi, M. Paoluzzi, N. Pellicciotta, A. Lepore, L. Angelani, and R. Di Leonardo, Generalized energy equipartition in harmonic oscillators driven by active baths, Phys. Rev. Lett. **113**, 238303 (2014).
[40] L. Dabelow, S. Bo, and R. Eichhorn, Irreversibility in active matter systems: Fluctuation theorem and mutual information, Phys. Rev. X **9**, 021009 (2019).
[41] A. Majhi, B. Das, S. Gupta, A. D. Ranjan, A. I. Mallick, S. Paul, and A. Banerjee, Decoding active force fluctuations from spatial trajectories of active systems, Phys. Rev. E **111**, 065411 (2025).
[42] U. Seifert, Entropy production along a stochastic trajectory and an integral fluctuation theorem, Phys. Rev. Lett. **95**, 040602 (2005).
[43] G. T. Landi and M. Paternostro, Irreversible entropy production: From classical to quantum, Rev. Mod. Phys. **93**, 035008 (2021).

[44] S. K. Manikandan, D. Gupta, and S. Krishnamurthy, Inferring entropy production from short experiments, Phys. Rev. Lett. **124**, 120603 (2020).

[45] S. K. Manikandan, S. Ghosh, A. Kundu, B. Das, V. Agrawal, D. Mitra, A. Banerjee, and S. Krishnamurthy, Quantitative analysis of non-equilibrium systems from short-time experimental data, Commun. Phys. **4**, 258 (2021).

[46] B. Das, S. K. Manikandan, and A. Banerjee, Inferring entropy production in anharmonic Brownian gyrators, Phys. Rev. Res. **4**, 043080 (2022).

[47] B. Das and S. K. Manikandan, Localizing entropy production along non-equilibrium trajectories, ArXiv:2503.20427.

[48] B. Das, S. K. Manikandan, S. Paul, A. Kundu, S. Krishnamurthy, and A. Banerjee, Irreversibility of mesoscopic processes with hydrodynamic interactions, Phys. Rev. E **112**, L023401 (2025).

[49] J. Li, J. M. Horowitz, T. R. Gingrich, and N. Fakhri, Quantifying dissipation using fluctuating currents, Nat. Commun. **10**, 1666 (2019).

[50] G. Nicoletti and D. M. Busiello, Tuning transduction from hidden observables to optimize information harvesting, Phys. Rev. Lett. **133**, 158401 (2024).

[51] J. Selimkhanov, B. Taylor, J. Yao, A. Pilko, J. Albeck, A. Hoffmann, L. Tsimring, and R. Wollman, Accurate information transmission through dynamic biochemical signaling networks, Science **346**, 1370 (2014).

[52] M. Bauer, M. D. Petkova, T. Gregor, E. F. Wieschaus, and W. Bialek, Trading bits in the readout from a genetic network, Proc. Natl. Acad. Sci. **118**, e2109011118 (2021).

[53] M. Kramar, L. Hahn, A. M. Walczak, T. Mora, and M. Coppey, Single cells can resolve graded stimuli, ArXiv:2410.22571.

[54] R. Quian Quiroga and S. Panzeri, Extracting information from neuronal populations: Information theory and decoding approaches, Nat. Rev. Neurosci. **10**, 173 (2009).

[55] G. Barzon, D. M. Busiello, and G. Nicoletti, Excitation-inhibition balance controls information encoding in neural populations, Phys. Rev. Lett. **134**, 068403 (2025).

[56] A. Lapolla and A. C. V. Godec, Faster uphill relaxation in thermodynamically equidistant temperature quenches, Phys. Rev. Lett. **125**, 110602 (2020).

[57] M. Ibánez, C. Dieball, A. Lasanta, A. Godec, and R. A. Rica, Heating and cooling are fundamentally asymmetric and evolve along distinct pathways, Nat. Phys. **20**, 135 (2024).

[58] M. Rose and S. K. Manikandan, Role of interactions in nonequilibrium transformations, Phys. Rev. E **109**, 044136 (2024).

[59] S. K. Manikandan, Equidistant quenches in few-level quantum systems, Phys. Rev. Res. **3**, 043108 (2021).

[60] M. Reinhardt, G. Tkačik, and P. R. Ten Wolde, Path weight sampling: Exact Monte Carlo computation of the mutual information between stochastic trajectories, Phys. Rev. X **13**, 041017 (2023).

[61] W. Endo, F. P. Santos, D. Simpson, C. D. Maciel, and P. L. Newland, Delayed mutual information infers patterns of synaptic connectivity in a proprioceptive neural network, J. Comput. Neurosci. **38**, 427 (2015).

[62] M.-C. Ho and F.-C. Shin, Information flow and nontrivial collective behavior in chaotic-coupled-map lattices, Phys. Rev. E **67**, 056214 (2003).

[63] M. Staniek and K. Lehnertz, Symbolic transfer entropy, Phys. Rev. Lett. **100**, 158101 (2008).

[64] H. Dickten and K. Lehnertz, Identifying delayed directional couplings with symbolic transfer entropy, Phys. Rev. E **90**, 062706 (2014).

[65] C. Sarra, M. Baldovin, and A. Vulpiani, Response and flux of information in extended nonequilibrium dynamics, Phys. Rev. E **104**, 024116 (2021).

[66] D. Lucente, M. Baldovin, F. Cecconi, M. Cencini, N. Cocciaglia, A. Puglisi, M. Viale, and A. Vulpiani, Conceptual and practical approaches for investigating irreversible processes, New J. Phys. **27**, 041201 (2024).

[67] M. P. Leighton and D. A. Sivak, Jensen bound for the entropy production rate in stochastic thermodynamics, Phys. Rev. E **109**, L012101 (2024).

[68] B. Das, S. Paul, S. K. Manikandan, and A. Banerjee, Enhanced directionality of active processes in a viscoelastic bath, New J. Phys. **25**, 093051 (2023).

[69] L. Hahn, A. M. Walczak, and T. Mora, Dynamical information synergy in biochemical signaling networks, Phys. Rev. Lett. **131**, 128401 (2023).

[70] A. Bérut, A. Imparato, A. Petrosyan, and S. Ciliberto, Stationary and transient fluctuation theorems for effective heat fluxes between hydrodynamically coupled particles in optical traps, Phys. Rev. Lett. **116**, 068301 (2016).

[71] A. Kraskov, H. Stögbauer, and P. Grassberger, Estimating mutual information, Phys. Rev. E **69**, 066138 (2004). We use the mutual information estimator “mutual info regression” available in scikit-learn, a PYTHON module.

[72] B. C. Ross, Mutual information between discrete and continuous data sets, PLoS ONE **9**, e87357 (2014).

[73] We use the transfer entropy estimator provided with Ref. [28] at https://github.com/thempel/information.

[74] U. Khadka, V. Holubec, H. Yang, and F. Cichos, Active particles bound by information flows, Nat. Commun. **9**, 3864 (2018).

[75] A. R. Poggioli and D. T. Limmer, Odd mobility of a passive tracer in a chiral active fluid, Phys. Rev. Lett. **130**, 158201 (2023).

[76] A. Pahi, K. R. Sahoo, B. Das, S. Paul, and A. Banerjee, Light-driven simultaneous active and diffusive behaviour of asymmetric microclusters using a photophoretic trap in air, J. Phys.: Photonics **7**, 035026 (2025).

[77] C. W. Lynn, C. M. Holmes, W. Bialek, and D. J. Schwab, Decomposing the local arrow of time in interacting systems, Phys. Rev. Lett. **129**, 118101 (2022).

[78] A. Suchitran and S. K. Manikandan, Tuning the kinetics of intracellular transport, ArXiv:2407.18784.

[79] S. Chennakesavalu, S. K. Manikandan, F. Hu, and G. M. Rotskoff, Adaptive nonequilibrium design of actin-based metamaterials: Fundamental and practical limits of control, Proc. Natl. Acad. Sci. **121**, e2310238121 (2024).

[80] M. P. Leighton and D. A. Sivak, Flow of energy and information in molecular machines, Annu. Rev. Phys. Chem. **76**, 379 (2024).

[81] D. Salambô, B. Besga, R. Mothe, D. Guéry-Odelin, E. Trizac, A. Petrosyan, L. Bellon, and S. Ciliberto, Engineered swift equilibration of brownian particles: consequences of hydrodynamic coupling, SciPost Phys. **9**, 064 (2020).

[82] D. Y. Kim, S. G. Nagella, K. H. Choi, and S. C. Takatori, Direct experimental measurement of many-body hydrodynamic interactions with optical tweezers, Phys. Rev. Fluids **10**, 064301 (2025).
[83] S. Oikawa, Y. Nakayama, S. Ito, T. Sagawa, and S. Toyabe, Experimentally achieving minimal dissipation via thermodynamically optimal transport, ArXiv:2503.01200.
[84] D. Villamaina, A. Baldassarri, A. Puglisi, and A. Vulpiani, The fluctuation-dissipation relation: How does one compare correlation functions and responses? J. Stat. Mech.: Theory Exp. **2009**, P07024 (2009).
[85] N. Ohga, S. Ito, and A. Kolchinsky, Thermodynamic bound on the asymmetry of cross-correlations, Phys. Rev. Lett. **131**, 077101 (2023).